

EVALUATION OF PERCEIVED X-15 FLYING QUALITIES BASED ON RAPID AERODYNAMIC PREDICTIONS

Hannes B. Rogers[1], Timothy T. Takahashi,[1] Jose A. Camberos[1] & Ramana V Grandhi[1]

[1]Air Force Institute of Technology, Wright-Patterson AFB, OH, USA

Abstract

In this paper we examine the utility of rapid aerodynamic prediction methods to support the design of high-speed vehicles. This is not a parameter identification paper. This is a study documenting how well a conceptual-design quality aerodynamic database can predict bare-airframe and augmented-control flying qualities of high-speed aircraft. In this work, we aerodynamically model the North American X-15 using a cocktail of vortex-lattice and empirical zero-lift-drag techniques. We then study its dynamical motions using equivalent-low-order systems analysis and time-domain non-linear simulations. We compare our computed motions with actual pilot reports from the X-15 program. We demonstrate that classical panel-method flow solvers provide sufficient quality data to replicate and predict essential flight behavior at many flight conditions.

Keywords: Flight Mechanics, Flight Test, Stability & Control, Modeling & Simulation, History

1. Introduction

The X-15 program marked a pivotal time in U.S. aviation history; it was the first piloted aircraft capable of hypersonic flight. It explored many aspects of high-speed flight, including aerodynamics, aerothermodynamics, materials, propulsion technologies and control issues related to high-speed flight within and beyond the atmosphere.

This paper investigates the impact of the pilot-selectable-gain Stability Augmentation System (SAS) used in early X-15 flights on its flight dynamics. While pen-plotter traces of flight motions by and large have not survived the ravages of time, the NASA flight test center at Edwards Air Force Base did archive pilot briefing and debriefing reports. Due to the unavailability of detailed time-history logs, we are unable to perform any sort of parameter identification study. However, qualitative pilot debriefing reports, which predate the modern test pilot Cooper-Harper vocabulary, do provide insight into both the bare-airframe and augmented flying qualities of the X-15 across its wide-ranging flight-envelope.

Our work here is to understand how well a lightly calibrated conceptual-design quality aerodynamic database can predict both bare-airframe and augmented control flying qualities of high-speed aircraft. In this work, we aerodynamically model the North American X-15 using a cocktail of vortex-lattice [1] and empirical zero-lift-drag [2] techniques. We then study its inherent dynamic motions using equivalent-low-order systems analysis and time-domain non-linear simulations.

This paper demonstrates that classical panel-method flow solvers provide sufficient quality data to replicate and predict the essential flight behavior of the X-15 both open-loop and closed-loop at many flight conditions.

2. The X-15

The X-15 program provided invaluable flight test data to support the Apollo and the STS (Space Shuttle) programs.

2.1 Historical Background

National Advisory Committee for Aeronautics (NACA) officially started the X-15 program. It had become apparent to many that hypersonic flight had military and commercial utility. The goal of the X-15 was to leverage earlier work and build a research aircraft to measure many parameters during high-speed flight: aerothermal heating and materials interactions, aerodynamic properties, propulsion system performance, as well as piloting command and control strategies. [3] The intent was to

complete airframe design and manufacturing within "a period of only about three years." This, in turn, made the use of new technologies and manufacturing techniques impossible [4].

The X-15 conceptual design process was an internal NACA study. The NACA decided to specify a conventionally configured wing/body/tail airframe to minimize issues with subsonic launch and landing. It was to be fit with all moving horizontal fins for pitch and roll and a variable wedge-angle vertical tail (dorsal and ventral) for yaw. NACA intended that the aircraft feature active stability augmentation (synthetic aerodynamic pitch, yaw and roll damping plus reaction control jets) to effectively control the aircraft within and beyond the atmosphere. The NACA desired an Inconel X hot-structure due to its favorable heat sink characteristics. Because the NACA was not in a position to manufacture an aircraft, they reached out to the Air Force and Navy to discuss joint requirements and find a suitable contractor who would could manufacture it. [4]

The government team selected North American Aviation as the prime contractor for the X-15. In total, three airframes were built for the flight test program (serial numbers 56-6670, 56-6671, and 56-6672). As the program matured, modifications were made to specific tail number aircraft arising from aircraft damage, flight test lessons learned (i.e., the removal of the large ventral fin), or from a desire to expand program scope (i.e., flights with the dummy scramjet engine). [4]

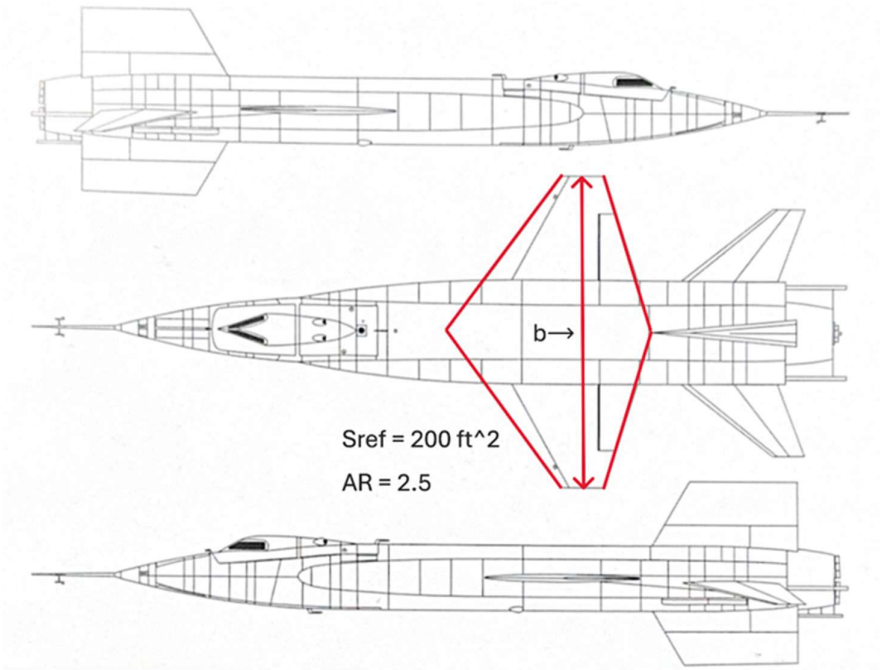


FIGURE 1 – Three View Drawing of the X-15-1 showing a detailed view of the geometric configuration of the aircraft. Note the trapezoidal wings with an aspect ratio of 2.5. Adapted from Ref. [5] Public Domain.

2.2 Aerodynamic Configuration

For this work, we analyze the initial, original configuration for X-15-1 (airframe 56-6670) as flown with the interim XLR-11 rocket motors; see FIGURE 1. [5] The geometric and physical properties of the X-15-1 are described in Ref. [5].

X-15 aerodynamic data is presented in customary aircraft stability-axis nomenclature. [6] It has a *Sref*=200-ft^2 trapezoidal planform wing with *b*= 22.36-ft span and $\bar{c}$=10.27-ft reference chord. [5] The wing has AR=2.5 and uses a modified NACA 66-005 airfoil with no dihedral and no spanwise twist. The empennage includes all moving horizontal tail fins (also using a modified NACA 66-005 airfoil) as well as 10^o wedge section dorsal and ventral vertical tails. Geometry may be found in TABLE 1.

The horizontal tail fins are somewhat smaller than the wings; total area is 115.45-ft^2. [5] In addition, the horizontal tails have a negative 15 °dihedral angle, in contrast with the 0 °of the wings. These all-moving fins are controlled by both the pilot and the SAS. The deflection limits differ considerably depending on their function. In pitch (longitudinal) the collective motion of the horizontal fins is limited to +15° and negative 35° regardless of pilot or SAS input. Roll control (lateral) of the horizontal tail, on the other hand, differentiated between the pilot and SAS commands. The pilot was given a range of ±15° whereas the SAS had twice the range at ±30°.

Both dorsal and ventral vertical tails are configured as 10° included angle wedges. [5] The dorsal tail was slightly larger with an airfoil section of 40.91-ft^2 compared to 34.41-ft^2 for the ventral tail. In addition, the rudder (movable surface area) of the dorsal tail was 26.45-ft^2 while the ventral tail had a rudder area of 19.95-ft^2. The upper and lower rudders are coordinated together to command yaw; their total range of motion is limited to ±7.5°. Both vertical tail sections would move in unison when the pilot or the SAS is the source of the command.

The fixed portion of the vertical fin wedge angle may be varied to provide a directional stability enhancing “speed-brake” action. [5] The speed brake was not employed for the missions we analyzed.

TABLE 1 – Geometrical Information for X-15-1. From Ref. [5]. Public Domain.

Wing:	
Airfoil section	NACA 66005 (Modified)
Total area (includes 94.98 sq ft covered by fuselage), sq ft	200
Span, ft	22.36
Mean aerodynamic chord, ft	10.27
Root chord, ft	14.91
Tip chord, ft	2.98
Taper ratio	0.20
Aspect ratio	2.50
Sweep at 25-percent-chord line, deg	25.64
Incidence, deg	0
Dihedral, deg	0
Aerodynamic twist, deg	0
Flap -	
Type	Plain
Area (each), sq ft	8.30
Span (each), ft	4.50
Inboard chord, ft	2.61
Outboard chord, ft	1.08
Deflection, down, deg	40
Ratio flap chord to wing chord	0.22
Ratio total flap area to wing area	0.08
Ratio flap span to wing semispan	0.40
Trailing-edge angle, deg	5.67
Sweepback angle of hinge line, deg	0
Horizontal tail:	
Airfoil section	NACA 66005 (Modified)
Total area (includes 63.29 sq ft covered by fuselage), sq ft	115.34
Span, ft	18.08
Mean aerodynamic chord, ft	7.05
Root chord, ft	10.22
Tip chord, ft	2.11
Taper ratio	0.21
Aspect ratio	2.83
Sweep at 25-percent-chord line, deg	45
Dihedral, deg	-15
Ratio horizontal-tail area to wing area	0.58
Movable surface area, sq ft	51.77
Deflection -	
Longitudinal, up, deg	15
Longitudinal, down, deg	35
Lateral differential (pilot authority), deg	±15
Lateral differential (autopilot authority), deg	±30
Control system	Irreversible hydraulic boost with artificial feel
Upper vertical tail:	
Airfoil section	10° single wedge
Total area, sq ft	40.91
Span, ft	4.58
Mean aerodynamic chord, ft	8.95
Root chord, ft	10.21
Tip chord, ft	7.56
Taper ratio	0.74
Aspect ratio	0.51
Sweep at 25-percent-chord line, deg	23.41
Ratio vertical-tail area to wing area	0.20
Movable surface area, sq ft	26.45
Deflection, deg	±7.50
Sweepback of hinge line, deg	0
Control system	Irreversible hydraulic boost with artificial feel
Lower vertical tail:	
Airfoil section	10° single wedge
Total area, sq ft	34.41
Span, ft	3.83
Mean aerodynamic chord, ft	9.17
Root chord, ft	10.21
Tip chord, ft	8
Taper ratio	0.78
Aspect ratio	0.43
Sweep at 25-percent-chord line, deg	23.41
Ratio vertical-tail area to wing area	0.17
Movable surface area, sq ft	19.95
Deflection, deg	±7.50
Sweepback of hinge line, deg	0
Control system	Irreversible hydraulic boost with artificial feel
Fuselage:	
Length, ft	50.75
Maximum width, ft	7.33
Maximum depth, ft	4.67
Maximum depth over canopy, ft	4.97
Side area (total), sq ft	215.66
Fineness ratio	10.91
Speed brake:	
Area (each), sq ft	5.37
Mean span (each), ft	1.60
Chord (each), ft	3.36
Deflection, deg	35
Frontal area at maximum deflection, sq ft	13.8
Base area (fuselage, side fairings, vertical fins), sq ft	31.18
Total frontal area (maximum) including wing and horizontal tail at 0° deflection, sq ft	38.8

2.3 Mass Properties

In addition to the geometric characteristics of the X-15, the stability of the aircraft is also influenced by its weight during flight and its associated mass moments of inertia. [7] At launch: W=32,700-lbm; Ixx~5,100-slug-ft^2; Iyy~107,600 slug-ft^2, Izz~109,300 slug-ft^2, Ixz=-1,100-slug-ft^2. Gliding and landing with all fuel consumed leads to: W=14,000-lbm; Ixx~3,600-slug-ft^2; Iyy~83,500 slug-ft^2, Izz~85,100 slug-ft^2, Ixz=-500-slug-ft^2. We follow NASA flight test procedure (see FIGURE 2) and linearly interpolate mid mission mass properties from this reference. [8] Consequently, there is considerable imprecision in knowing the actual weight and moments of inertia at the analyzed test points; this uncertainty may or may not have a significant impact on the dynamic stability of the aircraft.

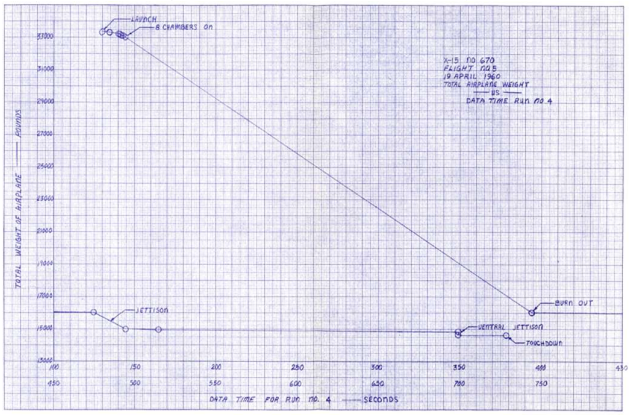


FIGURE 2 – Weight vs Time-history Chart (ex. From NASA supplied planning documents for X-15 Flight 1-5-10). Ref [8]. Public Domain.

2.4 Propulsion

One persistent challenge that was under parallel development with the X-15 aircraft design was the fact that there was no engine available that could meet all the requirements for the program. [4] As a result, Reaction Motors had been selected as the contractor to produce the XLR-99 engine that was to be integrated with North American Aviation's aircraft design. [4] However, the XLR-99 was delayed to such a degree that a replacement engine, the XLR-11, had to be used at the start of flight testing. [5] This was an older design, previously used on the Bell X-1. For early X-15 flights, North American integrated two XLR-11 engines into the X-15. Together, they provide ~16,000 lbf thrust at 60,000 ft altitude; see FIGURE 3. All flights analyzed in this paper were flown using the pair of XLR-11 engines. [7] The XLR-11 could not be conventionally throttled; thrust level was controlled by enabling or disabling one or more individual combustion chambers. [5][7]



FIGURE 3 – Two XLR-11 engines installed on the X-15-1 showing all 8 thrust chambers. Also shown are the dorsal and ventral vertical tails as well as the-15° dihedral angle of the horizontal tail. Ref [4]. Original image courtesy NASA. Public Domain.

2.5 Flight Control System

Due to the high speeds and altitudes at which the X-15 flew, a Stability Augmentation System was required for positive control; see FIGURE 4. The initial production X-15 SAS was designed by Westinghouse with simplicity and reliability in mind. It is a three-axis artificial damping SAS with body reference pitch, roll, and yaw channels. [9][10] It senses signals from three rate gyros and commands two pitch-roll servo cylinders (the collective / differential tailplanes) and a yaw servo-cylinder (the rudder). The pilot may control the level of synthetic damping through three (pitch, roll and yaw) independent gain selector knobs.

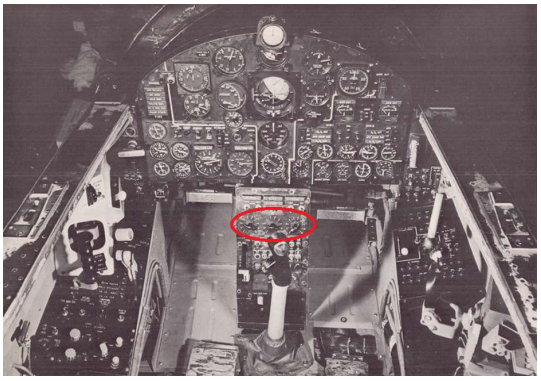


FIGURE 4 – X-15 cockpit showing instrumentation gauges as well as the gain selector switches right behind the center stick, shown in the red circle. Ref [10]. Public Domain.

The SAS also includes variable aileron-rudder-interconnect (designated YAR). It sends a signal from the yaw gyro to the roll channel. When engaged, the horizontal stabilizer positions are functions of sensed pitch, roll, and yaw rate of the aircraft.

A block diagram of the SAS may be found overleaf as FIGURE 5. Signals from each of the rate gyros are passed through the gain control blocks which amplifies the gyros sensed rates. The demodulator shaping bandpass filters the signal which is then passed to the servo-cylinder driver stage. The inputs given from the pilot and the signals sent from the SAS are combined to provide a single surface actuator deflection [9]

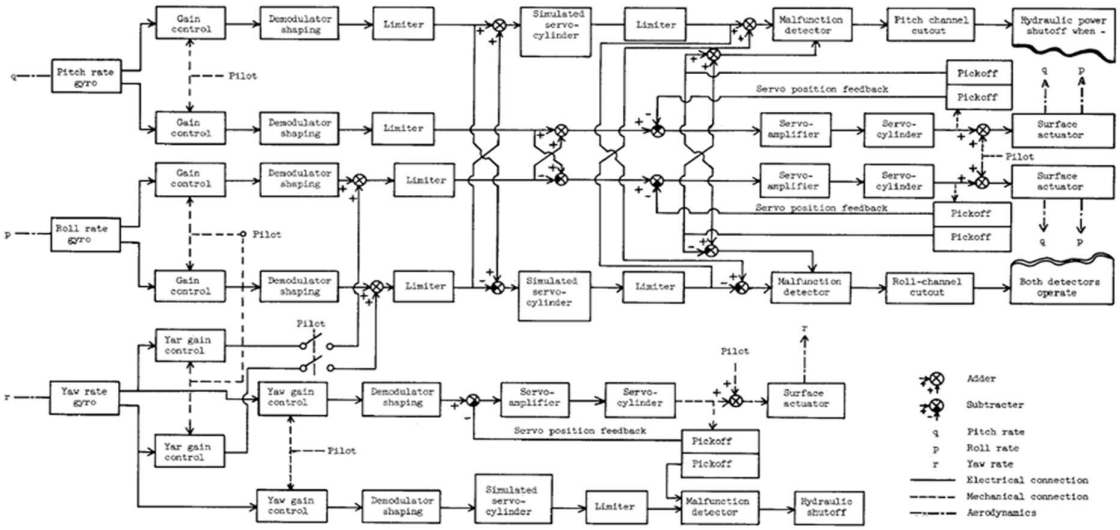


FIGURE 5 – X-15 Functional Block Diagram showing the components of the control system and how pilot inputs and signals from the SAS are transferred into surface deflections of the horizontal and vertical tails. Ref [9]. Public Domain

There are three gain selector switches, one for each directional channel, each of which is adjustable from gain settings 1-10. The gains for each setting are shown below in TABLE 2. We express the feedback gains in terms of engineering units (deg/deg/sec) and increase in magnitude as the gain selector setting is increased. If the gain selector switch setting is turned off, the associated gain value is also zero. [9]

Upon closer inspection of FIGURE 5, we see that while the pitch and yaw signals coming from the gain control blocks are added at the summing junction following the limiter in pitch and yaw, in the roll channel the gain and roll rate signal is instead subtracted at this point. Because the gains shown in TABLE 2 are all positive however, this negative sign becomes important when writing a modern time-step integrating simulation.

All the flights analyzed in this paper only operated with the pitch, roll, and yaw channels engaged. The YAR channel was either not used or not clearly annotated in the test cards and pilot report when trying to recreate the specific flights [9][10].

Table 2 – X-15 SAS Gains for Pitch, Roll, Yaw, and YAR. Data from Ref. [9]. Public Domain.

Gain Setting	Gain							
	Pitch		Roll		Yaw		Yar	
	Servo Cylinder	Surface	Servo-Cylinder	Surface	Servo-Cylinder	Surface	Servo-Cylinder	Surface
	In./deg/sec	Deg/deg/sec	In./deg/sec	Deg/deg/sec	In./deg/sec	Deg/deg/sec	In./deg/sec	Deg/deg/sec
1	0.005	0.075	0.0017	0.051	0.004	0.03	0.003	0.09
2	0.01	0.15	0.0033	0.1	0.008	0.06	0.006	0.18
3	0.015	0.225	0.005	0.15	0.012	0.09	0.009	0.27
4	0.02	0.3	0.0067	0.2	0.016	0.12	0.012	0.36
5	0.025	0.375	0.0083	0.25	0.02	0.15	0.015	0.45
6	0.03	0.45	0.01	0.3	0.024	0.18	0.018	0.54
7	0.035	0.525	0.0117	0.35	0.028	0.21	0.021	0.63
8	0.04	0.6	0.0134	0.4	0.032	0.24	0.024	0.72
9	0.045	0.675	0.015	0.45	0.036	0.27	0.027	0.81
10	0.05	0.75	0.0167	0.5	0.04	0.3	0.03	0.9

2.6 Aerodynamic Database

The X-15 was designed and flown during an era where wind tunnel data acquisition systems were immature. While wind tunnel data was collected at three NASA/LaRC and one NASA/ARC wind tunnel, the range of speeds and model orientation was limited. Many tested configurations were developmental, with noticeable variations from the flown aircraft. We found no surviving reports that document estimation of the X-15's aerodynamic dynamic derivatives (Cmq, Clp, Cnr). Given this history, we decided to build a lightly-calibrated aerodynamic database using two legacy early design codes, EDET and VORLAX.

VORLAX is a 1970's era computer program initially developed for NASA by Luis R. Miranda, Robert D. Elliot, and William M. Baker at the Lockheed-California Company. [1] It implements a generalized Vortex Lattice Method to calculate shock-free, attached flow at subsonic and supersonic flight conditions. [1] Over the years, co-author Takahashi and his associates have upgraded VORLAX to resolve minor algorithm deficiencies and to run better on modern computers. [11] This paper uses VORLAX version 2024d. [12] This code develops the aerodynamic coefficients for lift, induced drag and side forces as well as pitching, rolling and yawing moments all as functions of Mach number and angle of attack.

FIGURE 6 shows a top and oblique view of the X-15 model and highlights the different double-impermeable panels used to render the fuselage, wings, and horizontal stabilizers. The wedge shaped dorsal and ventral fins are modelled as pairs of inclined single-impermeable panels.

Because VORLAX is an inviscid potential flow code, it can only compute the component of drag

associated with pressure differentials. At supersonic speeds, the pressure fields are estimated presuming shock waves are firmly attached to panel leading and trailing edges.

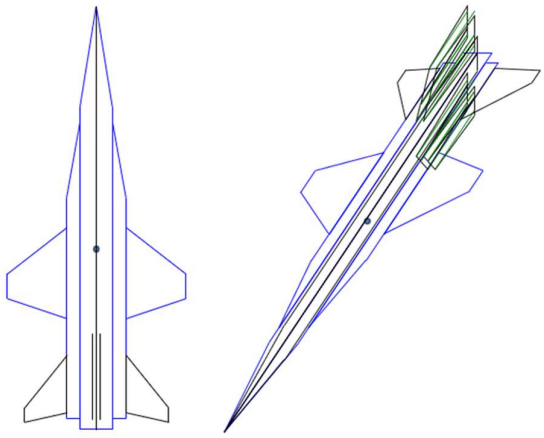


FIGURE 6 – Example VORLAX model used to generate the aerodynamic database for the X-15-1

In order to properly analyze the full aerodynamic characteristics of the X-15 we run VORLAX with control surfaces set to neutral and through various combinations of deflections (rudder deflected, horizontal collective, horizontal differential). Our linearized response to control surface deflections (i.e., *dCm/delev*) are based on a two-point derivative from maximum expected deflections. We also run VORLAX to predict dynamic derivatives (*Cmq*, *Clp*, *Cnr*) using its equivalent warped / twisted model capability.

Note that the static and dynamic stability derivatives calculated represent those of the bare airframe only and do not take into account any damping effects due to the SAS.

In order to account for zero-lift drag in the final calculations, we utilized the Empirical Drag Estimation Technique (EDET) program. It too was developed for NASA, this time by R.C. Feagin and W.D. Morisson also at the Lockheed-California Company. [2] This code has also been extended by co-author Takahashi to allow for drag estimation through Mach 5 and 300,000-ft. We have adjusted the "crud drag" factor to broadly match X-15 flight experience. [13]

The entirety of the aerodynamic database needed for time-domain simulation is seen over the following pages in FIGUREs 7 through 11. All data has been prepared in USAF customary stability axis. [6]

The estimated aerodynamic find the X-15-1 as broadly stable in pitch (*dCm/dCL*<0 from FIGURE 7c) and yaw (*dCn/d*β>0 from FIGURE 7e). The dihedral effect (*dCl/d*β from FIGURE 7f), on the other hand, fluctuates as the angle of attack changes. While the values are numerically small, they indicate that a positive sideslip may cause a roll to either left or right depending upon flight speed and attitude.

Elevator effectiveness (FIGURE 8a and 8b) tends to decline with increasing flight speed.

FIGUREs 9a and 9b show that the change in rolling moment coefficient due to a change in "aileron" deflection is relatively constant as angle of attack increases. The coefficients share the same sign; thus, the differential tail for "aileron" strategy features "proverse yaw" – a command to roll will yaw the aircraft into a turn.

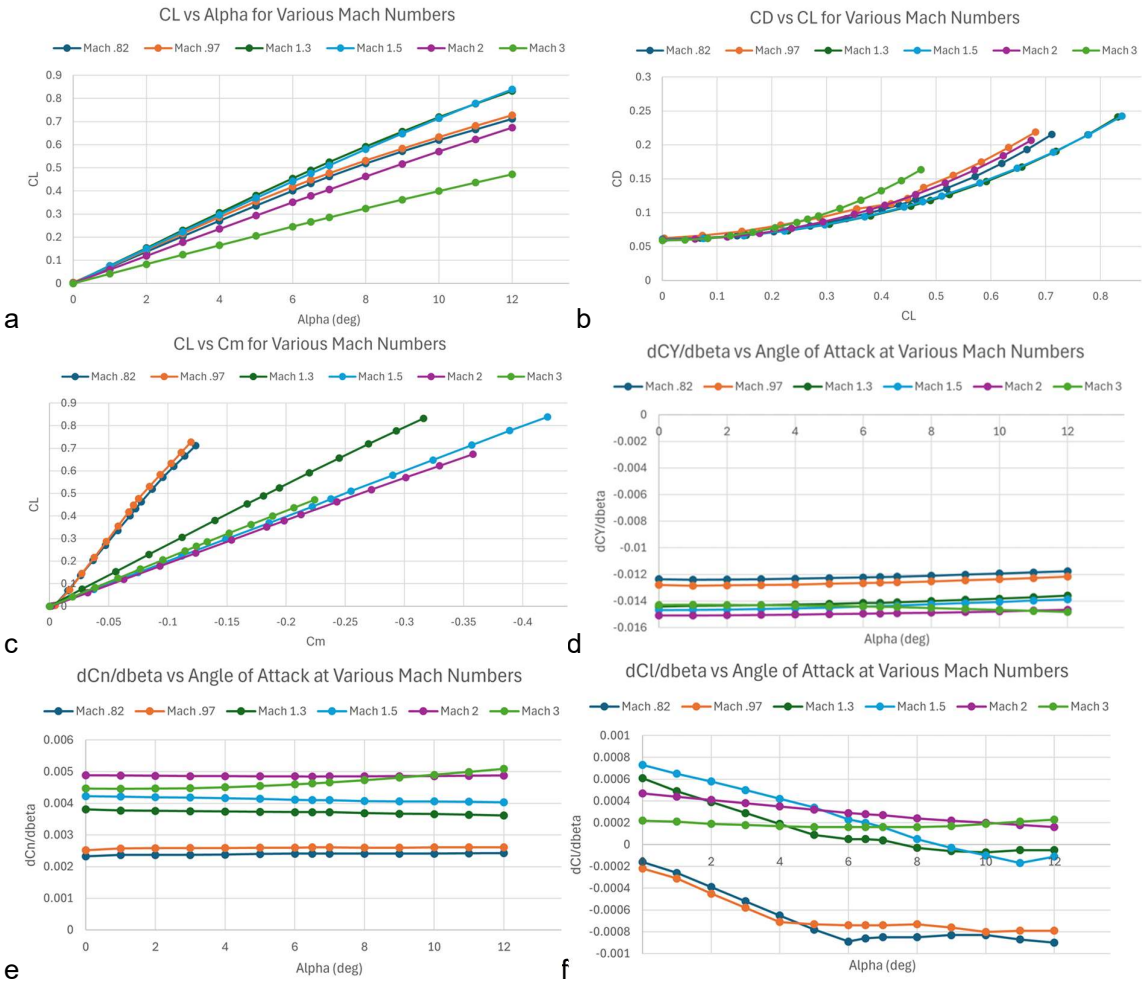


FIGURE 7 – X-15-1 Baseline Controls Neutral Aerodynamics from VORLAX/EDET cocktail. USAF Customary Stability Axis. a) CL vs vs α, b) CD vs CL, c) CL vs Cm, d) dCY/dβ vs α , e) dCn/dβ vs α, f) dCl/dβ vs α.

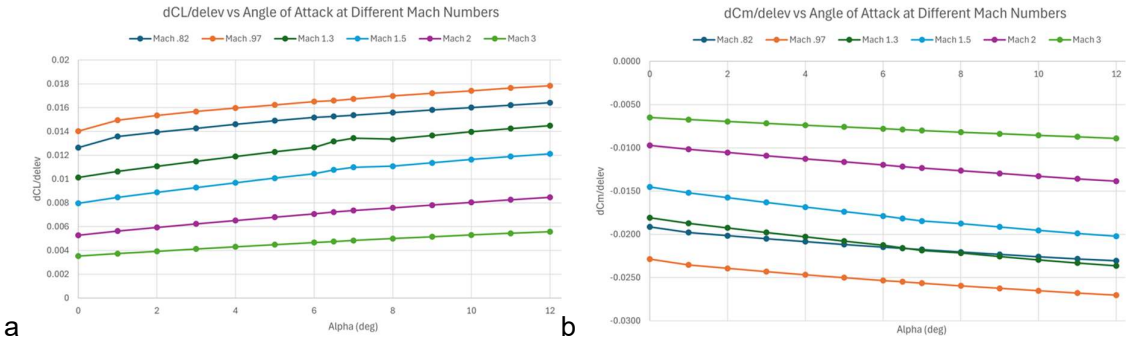
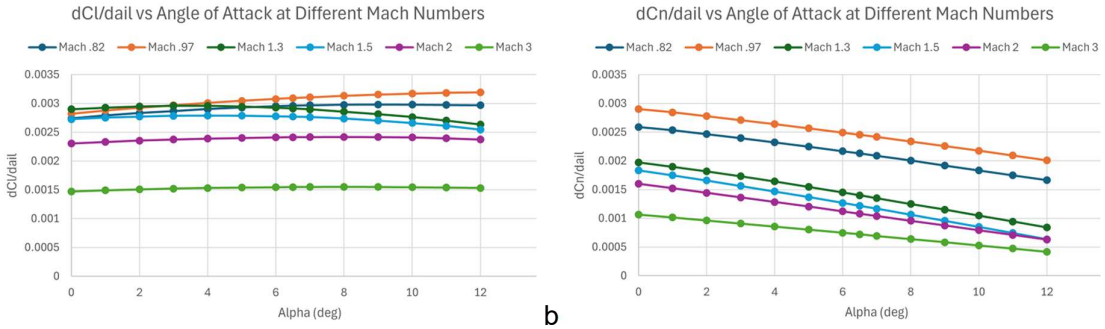
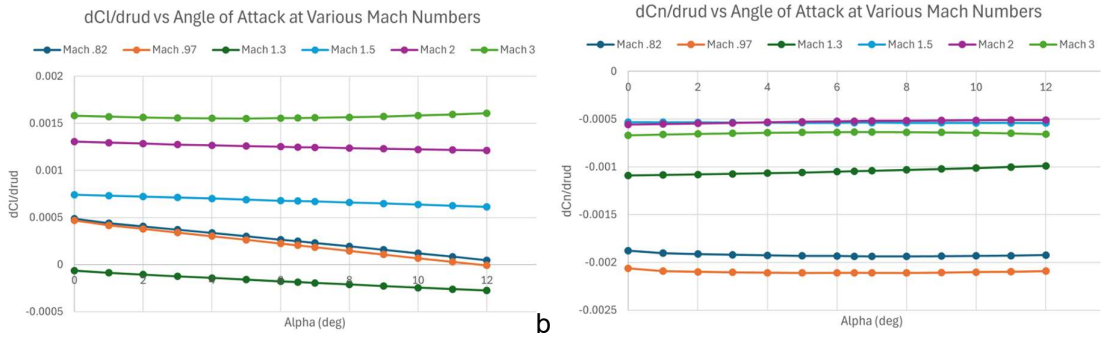


FIGURE 8 – Elevator Effectiveness (collective Horizontal Tail Deflections). USAF Customary Stability Axis. a) lift (*CL*) increments per unit collective fin deflection, b) pitching moment (*Cm*) increments per unit collective fin deflection



a b

FIGURE 9 - Aileron Effectiveness (differential Horizontal Tail Deflections). USAF Customary Stability Axis. a) rolling moment (*Cl*) increments per unit differential fin deflection, b) yawing moment (*Cn*) increments per unit differential fin deflection



a b

FIGURE 10 – Rudder Effectiveness (synchronized Dorsal and Ventral Tail Deflections). USAF Customary Stability Axis. a) rolling moment (*Cl*) increments per unit fin deflection, b) yawing moment (*Cn*) increments per unit fin deflection

FIGUREs 10a and 10b show considerable Mach number dependence to rudder effectiveness. Note the uniform yawing moment per degree of rudder deflection as a function of angle of attack. However, rudder effectiveness declines as speeds increase. The computations indicate that the rolling moment from the rudder tends to be adverse at all speeds except Mach 1.3, where it is marginally proverse.

Pilot comments on flying with the X-15's SAS show that it was effective in damping out motions of the aircraft in flight, especially at higher Mach numbers and altitudes where, in its absence, the expectation for severe oscillations increases. Of particular note were the recurring statements that damping in roll is especially important. Without synthetic damping in the lateral direction, the pilots noticed severe sensitivity in controlling the rolling motion of the bare aircraft. Flight test experience noted that this effect became worse as Mach and angle of attack increased. [9][14]

FIGURE 11 shows our estimates of the principal dynamic derivatives of the bare airframe. *Cmq* is always negative; which provides stabilizing pitch damping - its effectiveness declines with increasing Mach number. *Clp* is always negative; which provides stabilizing roll damping. *Cnr* is always negative; which provides stabilizing yaw damping. Note that the cross damping derivatives (*Cnp* and *Clr*) have strong Mach and angle-of-attack dependencies and change sign depending upon flight condition. Thus, the induced yaw-due-to-roll-rate may drive the sideslip positive or negative based on flight condition. Similarly, the presence of the large ventral is a factor which explains why the induced roll-due-to-yaw-rate may roll the aircraft left or right based on flight condition. Similarly, the large ventral tail has the effect of creating destabilizing rolling motions ($dCl/d\beta>0$) at high angles of attack, which again increased the need for effective damping across the entire flight envelope.

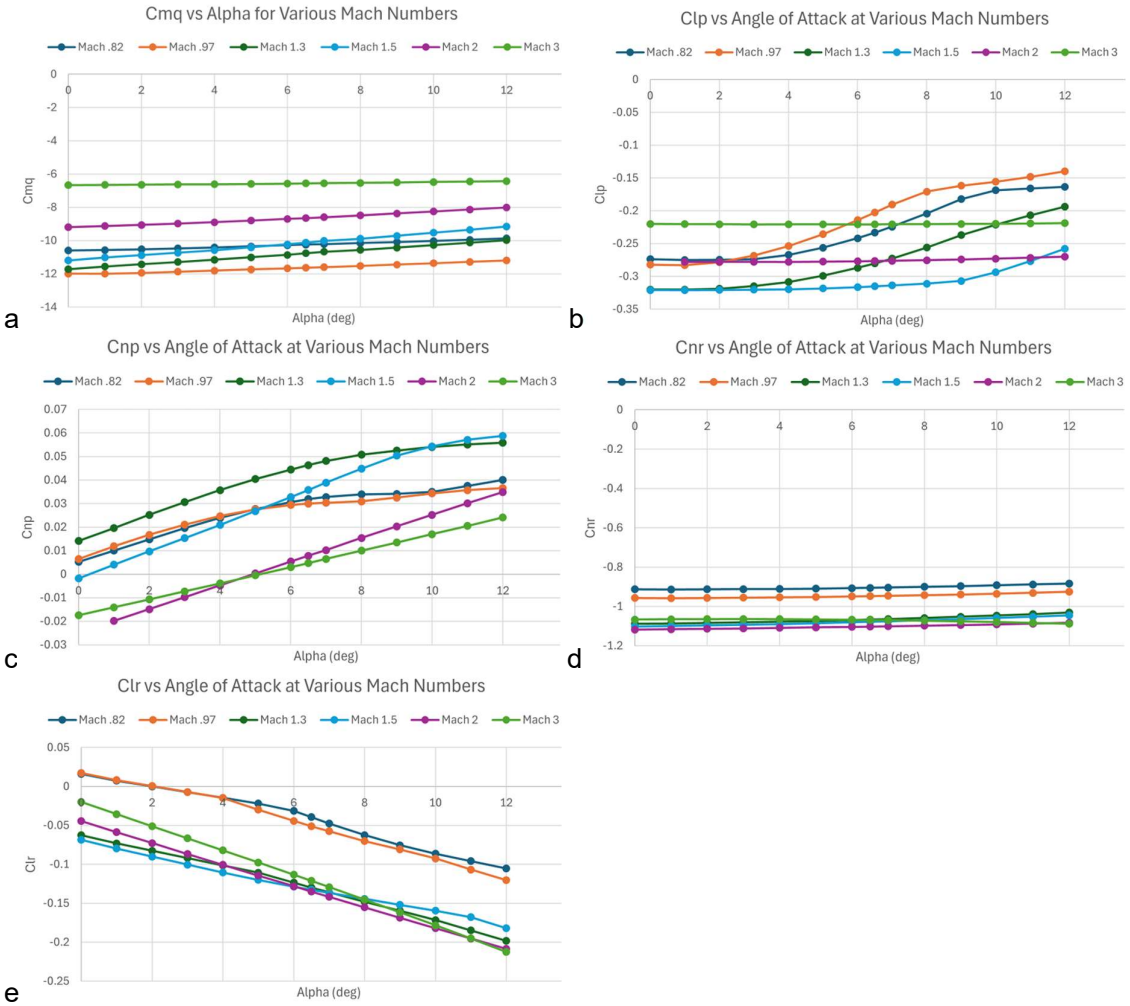


FIGURE 11 – Bare Airframe Dynamic Derivatives. USAF Customary Stability Axis.

3. Modelling & Simulation Approach

To thoroughly evaluate an aircraft's static and dynamic characteristics, we perform an analysis to see how it conforms to modern MIL-1797 or 8785C criteria. [15][16] The data described in Section II of this paper may be used to predict classical dynamic modes such as Dutch-Roll, Short-Period, and Phugoid as well as other coupled motions [19] to understand bare airframe behavior and the need, and practicality of closed-loop stability-augmentation and/or control-augmentation systems.

3.1 Equivalent Low Order Systems of Equations Used to Evaluate Stability

We first approach our assessment of the X-15 using an "equivalent low order systems" (ELOS) model based on 1- and 2-DOF simplification to the classical equations of motion and second, to a time-step integrating non-linear simulation based on the full classical equations of motion. We interpret our results in terms of modern MIL-STD-1797A / MIL-8785C criteria, which associates certain observed motions (frequencies, damping, excursions from trim) with "Cooper-Harper" type pilot descriptions and LEVEL 1,2 or 3 qualifiers. [15][16] A full description of our approach may be found in Rogers' complete thesis. [17] We also refer you to source documents in Takahashi, Griffin & Grandhi. [18] Our methods are broadly consistent with the formulation laid out in Yechout, et al. [19]

The X-15 SAS could "correct" unfavorable open-loop dynamics feed-forward (YAR) and feedback control laws; refer back to the block diagram in FIGURE 5). It used selectable fixed-gain feedback

to increase damping. We can model both the bare airframe and closed loop behavior using an "equivalent stability derivative" analysis paradigm, as advocated by McRuer and associates [20]. It computes augmented values of the various aerodynamic derivatives based upon linearized feedback gains; these were found in TABLE 2. Substitution of these values into the basic, stick-fixed equations provides a simple mechanism to estimate the frequencies and damping ratios associated with a closed-loop system with basic proportional feedback. [17][18]

Here, we illustrate how we use McRuer's method [20] to estimate the closed loop behavior of the X-15 using a quasi-static analysis.

For example, we may follow Ref. [18] and [19] to use the classical approximate Short-Period frequency and damping formulation:

$$\omega_{SP} \approx \sqrt{\frac{-57.3 \cdot \frac{\mathrm{dCm}}{\mathrm{d}\alpha} \cdot \bar{q} \cdot Sref \cdot \bar{c}}{Iyy}} \tag{1}$$

and:

$$\zeta_{sp} \approx -\frac{M_q + Z_\alpha / U_1}{2\,\omega_{sp}} \tag{2}$$

where the pitch angular acceleration due to pitch rate is:

$$M_q = C_{m_q} \frac{\bar{q}\, S_{ref} \bar{c}^2}{2\, Iyy\, VKTAS \left(\frac{6076}{3600}\right)} \tag{3}$$

and the normalized vertical acceleration due to angle of attack is:

$$\frac{Z_\alpha}{U_1} \approx -57.3 \frac{dCL}{d\alpha} \frac{\bar{q}\, S_{ref}}{\left(\frac{W}{g}\right) VKTAS \left(\frac{6076}{3600}\right)}. \tag{4}$$

and $VKTAS$ is the aircraft velocity in knots of true airspeed. [24]

Where *Sref* and $\bar{c}$ are intrinsic to the X-15. *W*, *Mach*, *Altitude*, *VKTAS*, $\bar{q}$ and *Iyy* are found from the post-test flight log. *dCL/dα*, *dCm/dα* and *Cmq* are found from the VORLAX aerodynamic database at the appropriate Mach number and attitude.

Pitch damping, as used in these equations, are functions of the bare-airframe damping, *Cmq**, and a pitch rate dependent gain setting (correlating the knob setting with the gain from TABLE 2) applied to the elevator:

$$C_{m_q}(M, \alpha) \approx C_{m_q}{}^*(M, \alpha) + \frac{dCm}{delev}\ 57.3\ K_{PITCHDAMP} \frac{q\ \bar{c}}{2\ VKTAS \left(\frac{6076}{3600}\right)} \tag{5}$$

MIL-1797A [15] and 8785C [16] assess Short-Period behavior in terms of the Control Anticipation Parameter (*CAP*) which gives preferred Short-Period characteristics as a function of pitch responsiveness:

$$\frac{n_Z}{\alpha} = \frac{57.3 \cdot q \cdot Sref \cdot \frac{dCL}{d\alpha}}{W} \tag{6}$$

The resultant criteria, $CAP = \frac{\omega_{sp}^2}{\frac{n_Z}{\alpha}}$. For general (Category B) flights, preferred LEVEL 1 flying qualities are associated when 3.6 > *CAP* > 0.085. Degraded LEVEL 2 flying qualities are associated with 10 > *CAP* > 0.038. If *CAP* < 0.038, pilots are likely to deem the flying qualities unacceptable.

Similarly, if we identify the ELOS Short-Period damping ratio, we can compare them against the quantitative ratings criteria found in MIL-1797A. Preferred LEVEL 1 flying qualities are associated with 2 > ζ_{SP} > 0.3; degraded LEVEL 2 flying qualities with 0.3 > ζ_{SP} > 0.2; poor LEVEL 3 flying qualities with 0.2 > ζ_{SP} > 0.15 and unacceptable flying qualities with ζ_{SP} < 0.15. [15]

We also address the Phugoid, Dutch-Roll, Roll-Mode and Spiral Divergence Modes. Phugoidal motions occur when an aircraft "wallows" and exchanges altitude and airspeed as it moves along its flight path. [24] Conversely the Dutch-Roll mode represents a lateral-directional oscillation of the aircraft. In flight, it is seen as a combination of wing rocking (changes in ϕ) and tail wagging (changes in β). The ϕ/β ratio determines the tendency to wing rock; as this ratio increases wing rock becomes more pronounced. [16] The Roll-Mode is a first-order response that characterizes the ability of an aircraft to respond to aileron input. If the time constant is too long, the aircraft is objectionably sluggish. Lastly, we may estimate the Spiral-mode; the tendency of an aircraft to either increase bank angle during a turn or to want to roll out of a turn. If this mode is sufficiently unstable, the flight path becomes difficult to control as it always wants to depart in a continuously tightening spiral motion. MIL 1797A and 8785C provide quantitative criteria to assess these motions as conforming to LEVEL 1,2 or 3 standards.

3.2 Time-Step Integrated 6-DOF Simulation Used to Evaluate Stability

We realize that Inner-loop augmentation is not all-powerful. Neither is the linearized "equivalent stability derivative" formulation, it implies an instantaneous, linear response of the aircraft to loop-closing control laws. This approach falls apart under two circumstances: first, when the control power lags commands through actuator-rate or other mechanical limits (group-delay and associated phase-shifts or mechanical resonances), and second, when the control surface saturates (either aerodynamically or by reaching its mechanical end-of-travel stops). The more unstable the bare-airframe, the greater the gain and the broader the bandwidth needed for successful loop closure. [21] Thus, successful loop closure is ultimately constrained by several factors: 1) the open-loop stick-fixed stability or instability, 2) the mass moments of inertia that govern how rapidly the vehicle responds to disturbances, and 3) the geometric limits to the aerodynamic authority of its control surfaces. When either rate or position limits are exceeded, no amount of feedback can mask a fundamentally unfavorable design.

To check against this, we also model the X-15 using a time-step integrating non-linear simulation. It integrates the classical aircraft equations of motion to compute a time-history of aircraft position (x,y,z) and motions (i.e. *α, b, ϕ, θ, P, Q, R, U, V, W, altitude, Mach, VKTAS*, etc.) which include pilot and SAS commanded control surface deflections. It imposes physical limits to control surface position and rates. In this work, we integrate the equations of motion with a 0.01-sec timestep.

All equations use a right-handed body (body axis) frame with +*X* forward, +*Y* right, and +*Z* up. Where rates appear in nondimensional form, conversions are carried explicitly; angles are stored/printed in degrees but differentiated in radians.

The simulation solves for Euler-angle rates at each time-step basis using the following equations:

$$\dot{\phi} = P + \tan(\theta)\left(Q\ sin(\phi) + R\ cos(\phi)\right) \quad (7)$$

$$\dot{\theta} = Q\ cos(\phi) - R\ sin(\phi) \quad (8)$$

$$\dot{\psi} = (Q\ sin(\phi) + R\ cos(\phi))/\cos\ (\theta) \quad (9)$$

Within the time-steps β and a evolve following the rate changes seen in the equations below:

$$\dot{\alpha} = \frac{U\dot{W} - W\dot{U}}{U^2 + W^2}, \quad (10)$$

$$\dot{\beta} = \frac{\dot{V}V_T - V\dot{V}_T}{V_T^2 \cos(\beta)} \quad (11)$$

$$V_T = \sqrt{U^2 + V^2 + W^2} \quad (12)$$

The force equations, which define the rate of translation, are:

$$\dot{U} = RV - QW - g_D \sin(\theta) + \frac{\bar{q}\ Sref\ (CL \sin(\alpha) - CD \cos(\alpha) + Thru}{m} \quad (13)$$

$$\dot{V} = -RU + PW + g_D \sin(\phi)\cos(\theta) + \frac{(Y_A + Y_T)}{m} \quad (14)$$

$$\dot{W} = QU - PV + g_D \cos(\phi)\cos(\theta) + \frac{Z_A + Z_T}{m} \quad (15)$$

The aerodynamic moments are dimensionalized from stability axis aero as:

$$L = qSrefb\left[\left(C_l + C_{lp}\left(\frac{b}{2U}\right)P + C_{lr}\left(\frac{b}{2U}\right)R\right)\cos(a) - \left(C_n + C_{np}\left(\frac{b}{2U}\right)P + C_{nr}\left(\frac{b}{2U}\right)R\right)\sin(a)\right] \quad (16)$$

$$M = qSref\bar{c}(C_m + C_{mq}\left(\frac{\bar{c}}{2U}\right)Q \quad (17)$$

$$N = qSrefb\left[\left(C_l + C_{lp}\left(\frac{b}{2U}\right)P + C_{lr}\left(\frac{b}{2U}\right)R\right)\sin(a) + \left(C_n + C_{np}\left(\frac{b}{2U}\right)P + C_{nr}\left(\frac{b}{2U}\right)R\right)\cos(a)\right] \quad (18)$$

Which feeds the full rotational rate equations:

$$\Gamma\dot{P} = I_{xz}\left[I_{xx} - I_{yy} + I_{zz}\right]PQ - \left[I_{zz}\left(I_{zz} - I_{yy}\right) + I_{xz}^2\right]QR + I_{zz}L + I_{xz}N \quad (19)$$

$$I_{yy}\dot{Q} = (I_{zz} - I_{xx})PR - I_{xz}(P^2 - R^2) + M \quad (20)$$

$$\Gamma\dot{R} = [I_{xx}(I_{xx} - I_{yy}) + I_{xz}^2]PQ - I_{xz}\left[I_{xx} - I_{yy} + I_{zz}\right]QR + I_{xz}L + I_{xz}N \quad (21)$$

where,

$$\Gamma = I_{xx}I_{zz} - I_{xz}^2 \quad (22)$$

Pitch, roll and yaw moment coefficients all include terms from bare-airframe, stick input and inner loop controller feedback.

$$Cm = Cm0 + \frac{dCm}{d\alpha}\alpha + \frac{dCm}{delev}\,\delta elev \quad (23)$$

$$Cl = \frac{dCl}{d\beta}\beta + \frac{dCl}{dail}\,\delta ail + \frac{dCl}{drud}\delta rud \quad (24)$$

$$Cn = \frac{dCn}{d\beta}\beta + \frac{dCn}{dail}\,\delta ail + \frac{dCn}{drud}\delta rud \quad (25)$$

Where

$$\delta elev = elev_{input} + K_{elev}\,q \quad (26)$$

$$\delta ail = ail_{input} + K_{ail}\,p \quad (27)$$

$$\delta rud = rud_{input} + K_{rud}\,r \quad (28)$$

The gain schedules correspond to the SAS knob position as defined in TABLE 2. [9][10] The pilot inputs were adjusted to match the simulator outputs with the pilot's flight report on how specific test point maneuvers were conducted and what the aircraft's response to those maneuvers was. We included control surface deflection limits to match the X-15-1 specifications of : horizontal tail limits are +15° and −35° for pitch and ±15° for roll and the vertical tail limits are ±7.5° for yaw. Because we did not know the actual actuator slew-rates, we did not impose rate limits for the X-15 in the code. [14] As a result, we cannot properly capture the high-frequency phase shifts which can drive Limit-Cycle-Oscillation at high gain settings.

4. Flight Test Points to Analyze

There were a total of 199 flights throughout the life of the X-15 flight test program. [4] The first test was flown on 6 June 1959, with the last being flown on 24 October 1968. This paper examines Flight 1-5-10, Flight 1-9-17, and Flight 1-11-21, all flown in 1960. [8][22][23] These XLR-11 powered flights were intended primarily as stability and control checkout flights to explore endoatmospheric supersonic operations; see FIGURE 12. All flights began with an air drop from the B-52 carrier aircraft around FL450 / *M*=~0.82. The highest planned flight altitude was ~78,000-ft. The fastest flight speed expected was *M*=~3.3. The peak dynamic pressure expected was $\bar{q}$ ~1,000-lbf/ft^2.

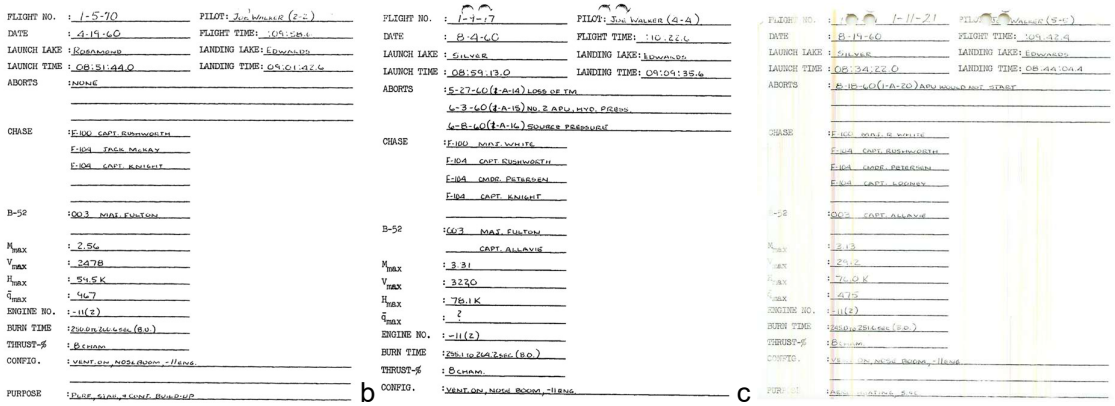


FIGURE 12 – X-15 Summary Coversheets for Flights Analyzed in this paper. a) 1-5-10, b) 1-9-17, c) 1-11-21. From Ref. [8][22][23]. Public Domain

From the surviving flight test planning documents, we follow the customary practice to linearly decrement the mass moments of inertia with fuel burn: *dIxx/dW* ~ 0.0802 slug·ft^2 / lbm; *dIyy/dW* = 1.1288 slug·ft^2 lbm; *dIzz/dW* = 1.294 slug·ft2 / lbm and *dIxz/dW* = 0.0321 slug·ft2/lbm.

Our first flight to correlate pilot comments to simulation was X-15-1 mission 1-5-10 from 19 April 1960; see FIGURE 13 (overleaf). [8] We can see that the SAS was engaged prior to air drop (knobs at 4, 4 and 8 - for pitch, roll and yaw). After drop, pilot Walker was to climb to M~1.5/ALT=60,000-ft, disable roll and yaw feedback and perform a rudder pulse during a 2-g turn – this would support bare-airframe parameter identification. The SAS would be re-engaged (knobs at 4,4 and 8), the aircraft would then roll out of the turn and while accelerating determine maximum trimmed sideslip (apply and sustain full rudder). The pilot would then disengage the yaw damper (knobs at 4,4,0) and make a second rudder pulse. After burnout, the pilot would hold α=10^o and perform a third rudder pulse with both roll and yaw dampers disengaged (knobs at 4,0 and 0) as well as a pitch pulse with the pitch damper disengaged and the roll and yaw dampers engaged (knobs at 0,4,8). The SAS gains would return to baseline (knobs at 4,4 and 8) for gliding approach and landing.

We are also able to access post test flight logs and debriefing notes for our flights; refer to FIGUREs 14, 15 and 16 (overleaf) for an example from X-15-1 mission 1-5-10. This information allowed us to better understand the X-15's weight, mass moments of inertia, speed and altitude across its "as-flown" mission. The surviving logs allow us to best estimate the actual conditions Pilot Walker experienced as he executed the various test points. When flight conditions are given in terms of Mach and Altitude, we presume that the altitude is the pressure altitude and that the true airspeed (VKTAS) and dynamic pressure ($\bar{q}$) can be inferred using the 1962 Standard Atmosphere. This work does not make any adjustments for flight in non-standard day conditions. The logs give us enough information to infer the angle-of-attack (α), bank angle (ϕ), acceleration (*dV/dt*) and flight path angle (θ) to reasonable accuracy.

We must note that the X-15 program test pilot comments regarding dynamic motions pre-date the establishment of Cooper-Harper ratings standards. Thus, we must take pilot observations as qualitative and subjective descriptions rather than as a code-phrase to describe a particular dynamic motion.

FLIGHT REQUEST
X-15 #670

Flight No. 5

Date of Request 4/13/60
Scheduled Date of Flight 4/19/60

Subject of Test: Performance, Stability and Control Build-Up

Airplane Configuration: Basic X-15 with stiffened side-fairing panels.

Engine Identification: XLR-11 (2 engines)

Launch: M = 0.82, H = 45K, SAS 4, 4, 8 at Waldrip on magnetic heading of 65°.

1. After launch, light 8 chambers and rotate to 8° α.
2. Maintain 8° α climb to 60K. (Minimum V_i = 260 knots).
3. At M = 1.5, 60K, perform turn to 15° α (2.0g). With SAS 4, 0, 0, perform rudder pulse during turn.
4. SAS 4, 4, 8, roll out of turn on magnetic heading of 310°. (Saltdale Lake).
5. During acceleration at 60K perform:
   (a) SAS: 4, 4, 8, full rudder deflection sideslip.
   (b) SAS: 4, 4, 0, rudder pulse.
6. SAS: 4, 4, 8. After burn-out (M = 2.2 to 2.5) initiate 10° α (2.0g) left turn and perform: (a) SAS 4, 0, 0 rudder pulse. (b) SAS 0, 4, 8 pitch pulse.
7. SAS: 4, 4, 8. Roll out on heading to high key.
8. During subsonic glide evaluate SAS off handling characteristics.
9. Landing: SAS 4, 4, 8, approach speed 300 knots, jettison ventral, turn on landing gear instrumentation, flaps and gear down.
10. Before APU shutdown, cycle controls, retract flaps and set stabilizer trim to zero.

FIGURE 13 - Flight Test Card for flight 1-5-10 showing X-15 release conditions and all test points from release to landing. Note the angles of attack, altitudes, Mach numbers and gain settings called out for each test point [8]. Public Domain.

670
X-15 FLIGHT 5

Prime to drop 38 sec. Drop to cylinder on 4 sec. Total prime 42 sec.

Starting Sequence	Time	ΔT	No. Cyls on	ΔCyl sec.	Total Cyl sec	P_c	A/W	LO_2	H_2O_2
upper 1 2 3 4 lower 1 2 3 ④ on/off	133.9								
upper 1 2 3 4 lower 1 ② 3 4 on/off	134.1	.2	1	.2	.2		4.075	4.20	.412
upper 1 2 3 4 lower 1 2 ③ 4 on/off	139.8	5.7	2	11.4	11.6		8.150	8.40	.447
upper 1 ② 3 ④ lower 1 2 3 4 on/off	140.3	.5	3	1.5	13.1		12.225	12.60	.486
upper 1 2 3 4 lower ① 2 3 4 on/off	141.8	1.5	5	7.5	20.6		20.325	21.30	.927
upper 1 2 ③ 4 lower 1 2 3 4 on/off	142.4	.6	6	3.6	24.2		24.390	25.50	.962
upper ① 2 3 4 lower 1 2 3 4 on/off	144.2	1.8	7	12.6	36.8		28.440	29.850	.995

FIGURE 14 - Time and sequence for engine chamber start after release for flight 1-5 10. Note the total time required (10.3 seconds) for the pilot to start all eight engine chambers. Ref. [8]. Public Domain.

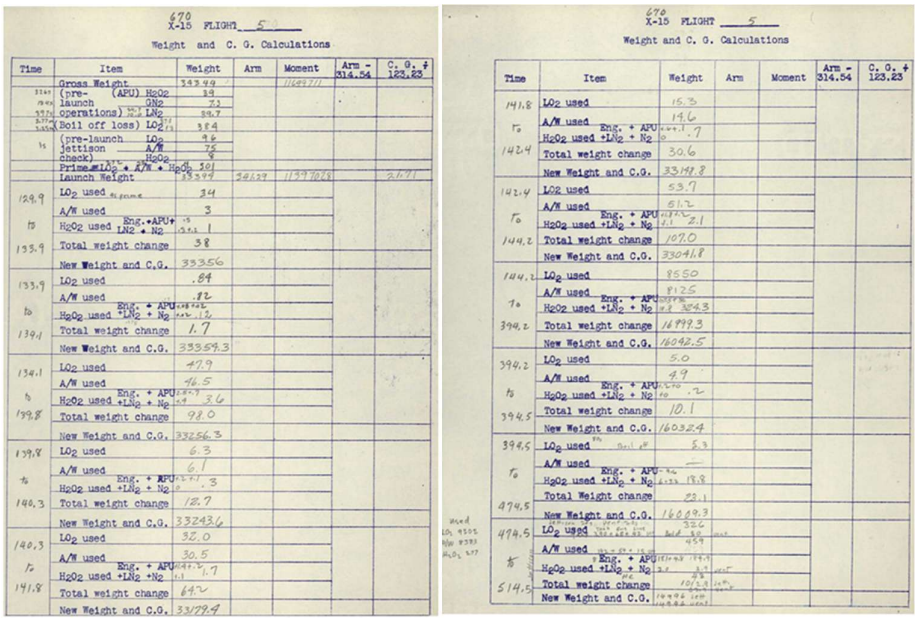


FIGURE 15 - Time and weight change for each engine chamber start after release as well as the time and weight change for the powered portion of flight 1-5-10. Note the launch weight of the X-15 found in the third block of time steps on the FIGURE on the right (Time: 144.2s to 394.2s). From Ref [8]. Public Domain.

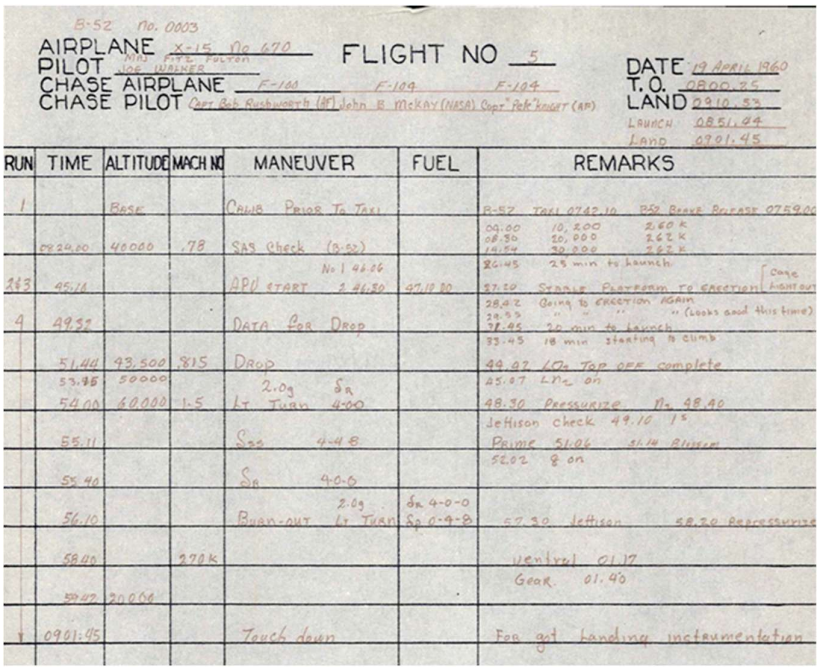


FIGURE 16 – As Flown report from flight 1-5-10. Note the column indicating the time at which specific maneuvers were executed along with the supplemental information on Mach and altitude. From Ref [8]. Public Domain.

4.1 Reconstruction of Events During Flight 1-5-10

FIGURE 17 (overleaf) shows the aircraft's dynamic response shortly after release. We selected the initial angle of attack (α=ϕ=0º) with β= 0.1° to introduce a small disturbance after release. The pilot logs (FIGURE 18, overleaf) notes an initial lateral stick deflection of "1-1/2 inches" pre-set before release; δail=−1.5°. The SAS gain knobs were set at 4,4,8. After release, the simulation was set up to position the aircraft at α=8° (trims with δelev=−4.29°). In order to reverse the roll experienced after release, δail=1.0° set as a final deflection. This command has the simulation reversing an initial left roll with wings level at the end of the run; consistent with pilot's comments.

The simulation ran for 11-sec to capture the time it took to start all 8 engine chambers (10.3-sec per flight log). We see in FIGURE 17 how the angle of attack increases to α~ 8° with a well-damped response (ζ_{SP}~0.51, LEVEL 1).The aircraft ends in a wings level state; sideslip and yaw rate perturbations are also present. The output shows a weakly damped (ζ_{DR}~0.15, LEVEL 2) response in sideslip angle and a reverse in yaw rate once minimal rudder is applied. Phugoid, Spiral and Roll Modes are all predicted to be favorable (LEVEL 1). There were no initial or final rudder deflection inputs however, the output shows rudder deflections as a result of gain settings and inherent yaw rate. We believe our simulation closely matches pilot experience.

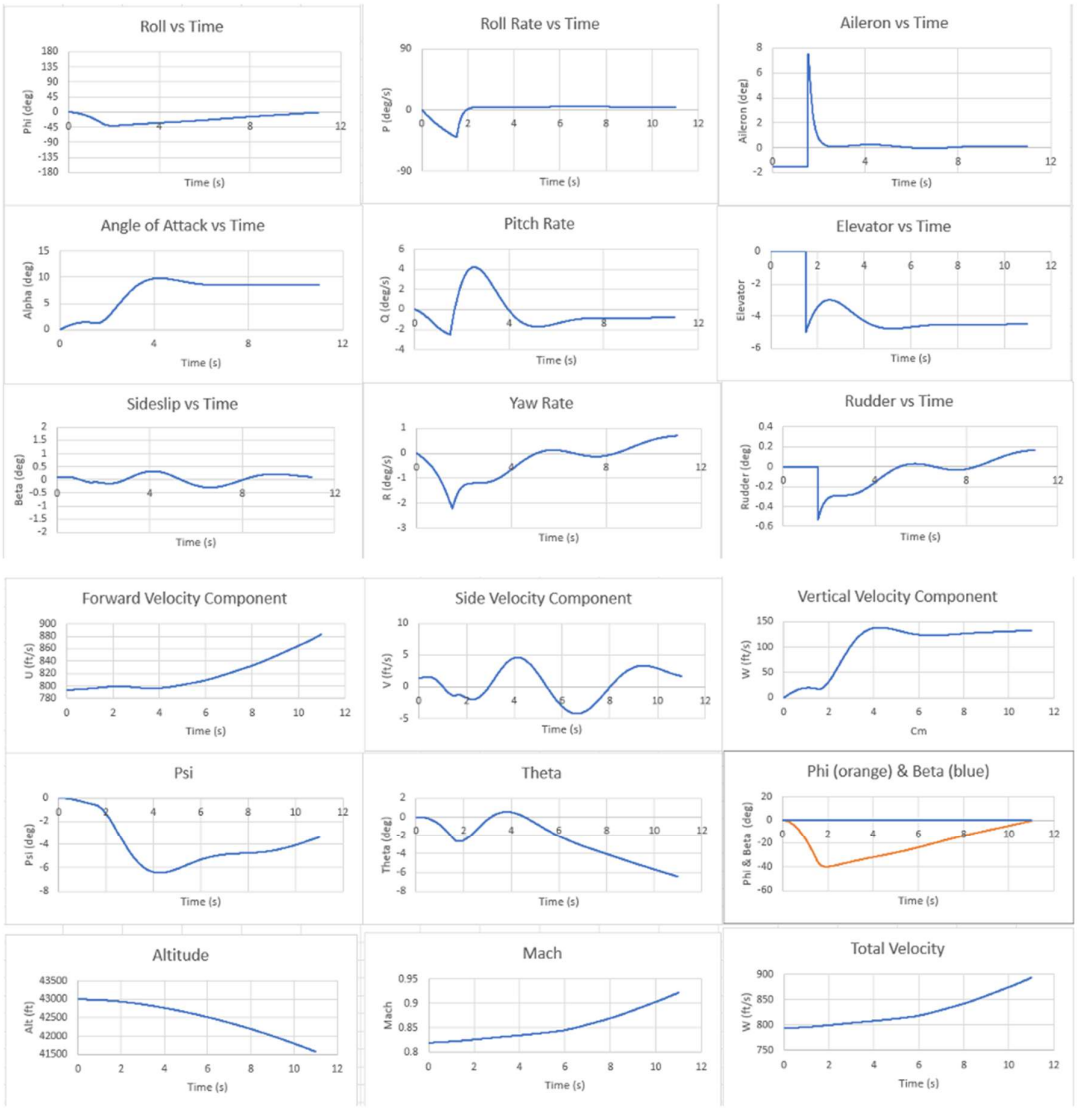
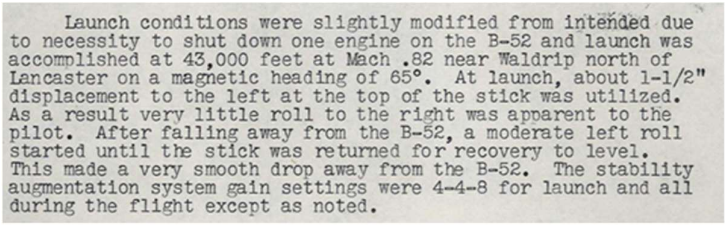


FIGURE 17 - Aircraft response during the release of the X-15 for flight 1-5-10. Note the change in angle of attack due to the elevator deflections as well as the small movements of the aileron and rudder to maintain trimmed flight conditions. Note the decrease in altitude as well as the phi to beta ratio plot showing the change in bank angle and sideslip due to control surface deflections.



Launch conditions were slightly modified from intended due to necessity to shut down one engine on the B-52 and launch was accomplished at 43,000 feet at Mach .82 near Waldrip north of Lancaster on a magnetic heading of 65°. At launch, about 1-1/2" displacement to the left at the top of the stick was utilized. As a result very little roll to the right was apparent to the pilot. After falling away from the B-52, a moderate left roll started until the stick was returned for recovery to level. This made a very smooth drop away from the B-52. The stability augmentation system gain settings were 4-4-8 for launch and all during the flight except as noted.

FIGURE 18 – Pilot debriefing notes for the release portion of flight 1-5-10. Note the comments about the initial lateral stick deflection and the ensuing roll that was experienced until the stick was returned to a neutral position. From Ref. [8]. Public Domain.

We next consider the push over at the end of the climb, which pilot Walker executed at Mach 1.4 and 58,500 ft. For this scenario, the initial angle of attack and flight path angle were set at 8° and 22° respectively. The initial elevator $\delta elev$=−16.45° to match the correct angle of attack. In order to model the pushover to represent a smooth leveling out at 60,000 ft the final elevator deflection was set to $\delta elev$=+3°. FIGURE 19 shows the change in angle of attack and pitch rate having a moderately damped response (ζ_{SP}~0.26, LEVEL 2). It also shows the aircraft leveling off at 60,000 ft. Additionally, the X-15 reaches this altitude before reaching Mach 1.5, which also corresponds with the pilot having to accelerate to this speed before proceeding with the next test point. This maneuver matches pilot commentary (FIGURE 20) which describes satisfactory "positively damped" response in all three axes.

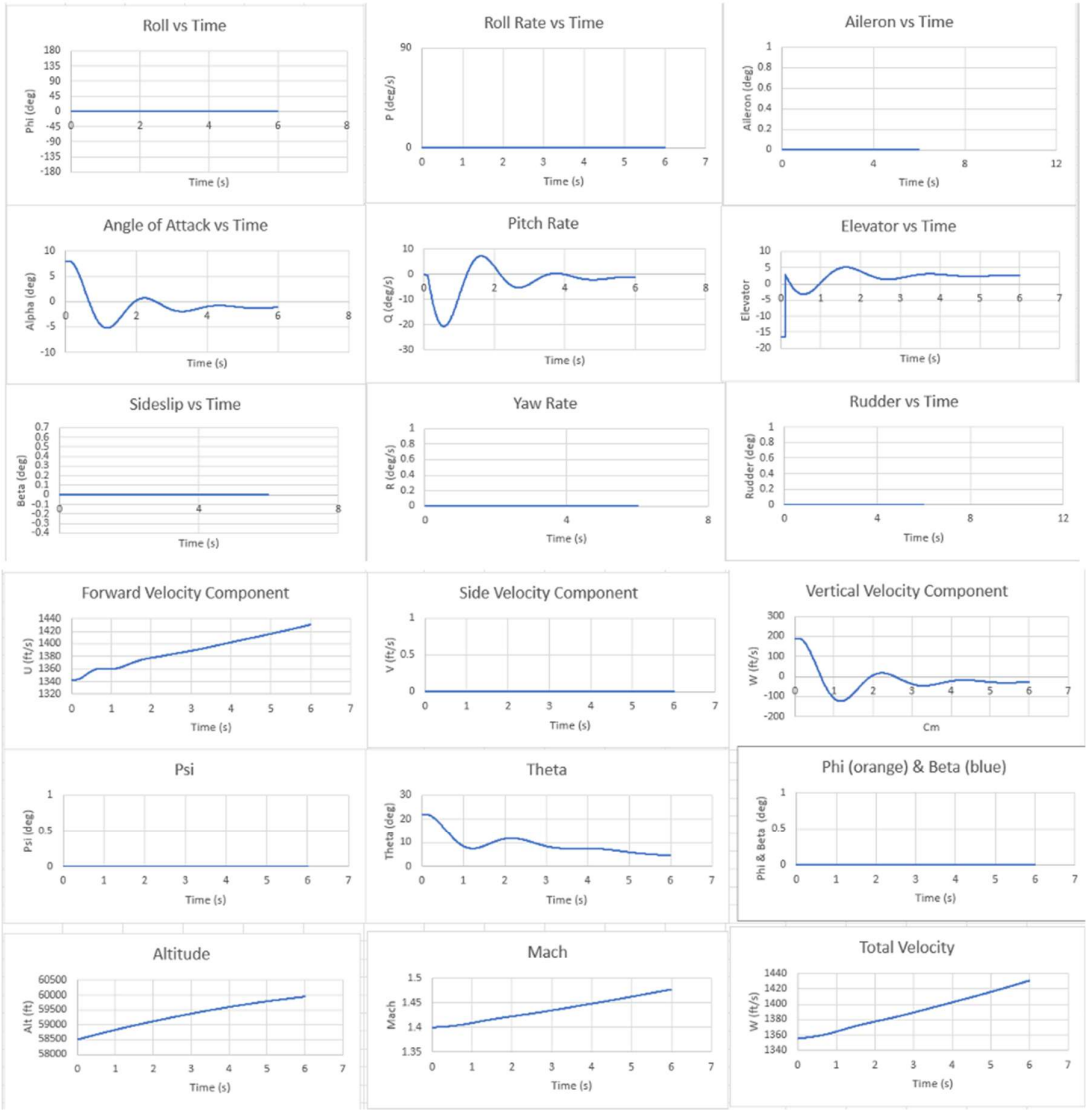


FIGURE 19 - Aircraft response at for the end of climb and pushover to level out at 60,000 ft. Note the damped response in pitch and change in angle of attack as the desired altitude is reached. Velocity, altitude, and flight path angle vs time for the pushover to 60,000 ft at the end of the climb for flight 1-5-10.

Upon reaching almost 59,000 feet round out to level at 60,000 feet was accomplished and acceleration to 1.5 Mach number instituted. At this speed a left turn to 15° angle of attack was established. At a steady 15° angle of attack the roll and yaw SAS channels were turned off and a left rudder pulse was performed. The aircraft appeared to be positively damped in the motions following the pulse. Roll and yaw were turned back on and the turn continued until the heading towards Saltdale was obtained.

FIGURE 20 - Pilot's comments u on leveling out at 60,000 ft and accelerating to Mach 1.5 before initiating the left turn and executing a rudder pulse with roll and yaw dampers turned off. From Ref. [10]. Public Domain.

To assess the effectiveness of the SAS, we zeroed its gains in the simulation. Turn next to FIGURE 21 to see the bare-airframe response under identical starting conditions. With only the inherent aerodynamic damping, the simulation shows significant pitching oscillations. While the motion isn't divergent, it is so lightly damped that its response would be considered LEVEL 3.

Additionally, the pushover can be modeled using McRuer inspired equivalent damped derivatives rather than using gain settings. FIGURE 22 shows the same pushover using the equivalent damped coefficients of *Cmq*, *Cl*p, and *Cnr* based on the feedback level indicated by knob position. The response of the aircraft in this scenario shows an almost identical response of the aircraft as that seen with the actual non-linear feedback laws applied; compare FIGURE 19 to FIGURE 22. This demonstrates the effectiveness of McRuer's methods for analysis provided that the gains are low enough to prevent control saturation and/or Limit-Cycle-Oscillation.

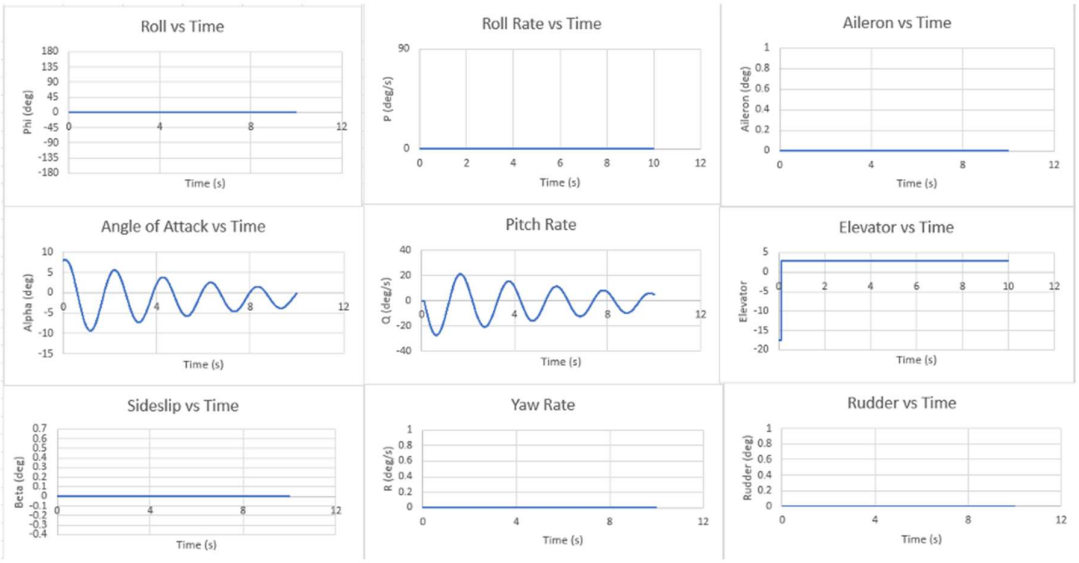


FIGURE 21 – Bare-Airframe response to the pushover to 60,000 ft. Note the lightly-damped response in pitch due to elevator deflection

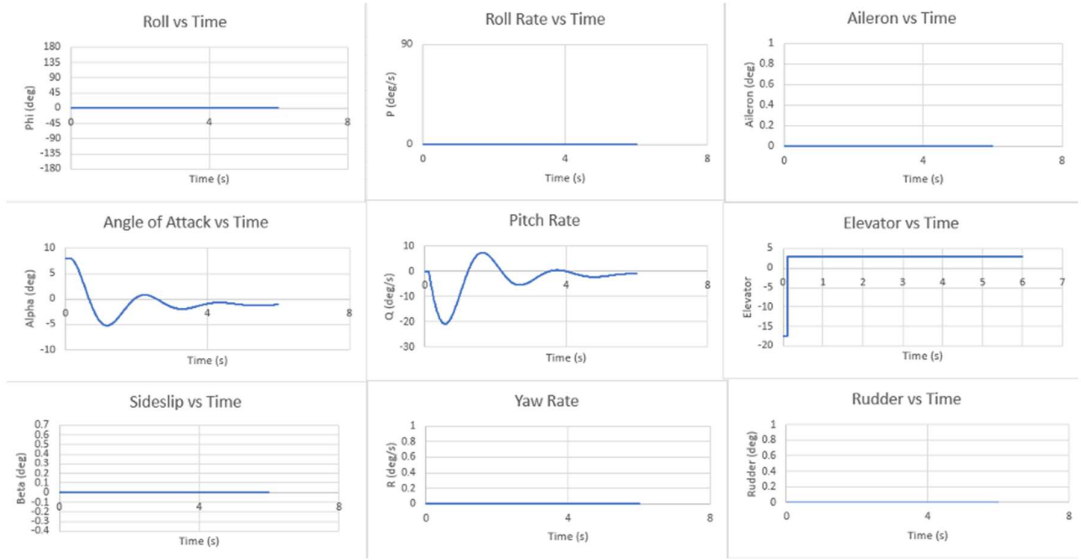


FIGURE 22 – Non-linear time-domain simulation using McRuer-style "Equivalent Stability Derivatives" in lieu of close-loop feedback.

The rest of this paper will summarize results found in principal author Rogers' thesis. [17]

The next evaluated flight test point was Mach 1.5, *nZ*=2 turn at ALT=60,000-ft with the SAS dampers engaged. Simulation shows motions well behaved. Pilot commentary indicated no adverse behavior.

The pilot was to then disable roll and yaw damping and apply a rudder pulse. The flight simulation shows damped (ζ=~0.3 behavior) in the pitch channel and moderate damping (ζ~0.1) in the Dutch-Roll. This is consistent with pilot reports that "the aircraft appeared to be positively damped in the motions following the pulse." [8]

A further test point involved holding full rudder at Mach 2, *nZ*=1 and ALT=60,000-ft with the SAS dampers engaged. As noted by the pilot, coordinating the skid requires a small amount of aileron; we agree, as the simulation needed δail~-4°. Pilot notes reported "4° to 5° sideslip," which generally matches with the simulator's output which peaks around β~4° then damps to a steady β~2° by the end of the 12 second run. The pitching motion is well-damped with a small oscillation before an essentially steady angle of attack is achieved.

The final test point analyzed for this flight was an attempted rudder pulse at Mach 2.5, *nZ*=1 and ALT=57,000-ft with the gain settings at 4,0,0. The simulation finds the vehicle divergent in roll., which is corroborated by pilot comments which noted that he could not actually perform the intended rudder pulse due to excessive residual oscillations.
In summary, our analysis of the as-flown flight test points using the Vortex-Lattice derived aerodynamic data feeding the flight simulator with defined feedback gain levels largely matched reported pilot observations. We also note that even with the feedback system engaged, the X-15 did not exhibit modern LEVEL 1 flying qualities at all times.

4.2 Reconstruction of Events During Flight 1-9-17

X-15-1 flight 1-9-17 requested the pilot to conduct two pitch pulses with the pitch gain settings turned off. [22] During the climb, the first pitch pulse was conducted at Mach 1.6 and ALT=60,000 ft and the second at Mach 2.0 and ALT=70,000-ft.

For both cases the simulation shows that the pitch pulse excited lightly damped oscillations which continue throughout the 10 second run. As expected, as flight speeds increase the bare-airframe damping grows weaker. This aligns with pilot's comments that the pitch pulse at Mach 1.6 was "moderately damped" and "lightly damped" at Mach 2. Both simulation and pilot comments noted that the pitching oscillations did not excite any appreciable lateral-directional dynamics. [22]

X-15-1 flight 1-9-17 also requested the pilot to perform a 3.8-gee pull up maneuver after fuel exhaustion. Our simulations show that with the lateral-directional SAS gains selected, flight where α>10° excites weakly damped Dutch-Roll behavior. This is consistent with pilot observations (see FIGURE 23) where directional oscillations became apparent only at high angle of attack.

As soon as level pitch attitude was obtained the aircraft was held at 1/2 "g" for the remainder of the powered flight and a gradual increasing dive angle was obtained during the course of acceleration to maximum speed. During this phase the airplane felt very good about all axes with a very small tendency toward minute lateral residual oscillation. However, this was so small as to be of no consequence as far as control of the airplane was concerned. Burnout occurred at slightly over indicated Mach 3.5. The 5 second coast at 1/2 "g" was carried out, then pullup to 4 "g" was initiated. The airplane responded with good control as the load factor increased. At about 3.8 "g" a noticeable tendency to small oscillation directionally was observed and in response to this indication, 3.8 "g" was the maximum pullup load factor. Then the nose was lowered and 1 "g" flight maintained from that point on as we were about level.

FIGURE 23 - Pilot report on the 3.8g pull up for flight 1-9-17. Note the statements about small directional oscillations once the aircraft experienced its maximum load factor. From Ref. [22]. Public Domain.

4.3 Reconstruction of Events During Flight 1-11-21

This flight was also piloted by Joe Walker with a planned top speed of M~3 and peak altitude of 70,000-ft; see Ref. [23]. The aircraft exhibited severe lateral-directional oscillations after burnout with the yaw and roll dampers disables (SAS gains at 4,0,0). The record shows additional post-flight analysis was

performed in 1960 to understand what the pilot experienced.

As with the other flights, both simulation and pilot reports indicate well damped behavior (ζ_{SP}~0.6 – LEVEL 1, ζ_{DR}~0.15 – LEVEL 2) at launch.

During initial climb, simulation and pilot reports indicate well damped behavior (ζ_{SP}~0.8 – LEVEL 1, ζ_{DR}~0.15 – LEVEL 2).

After burnout, with the roll and yaw damper gains set to zero, both simulation and pilot experiences indicate satisfactory Short-Period but very weak Dutch Roll damping. (ζ_{SP}~0.4 – LEVEL 1, ζ_{DR}~0.03 – LEVEL 2). The simulation (see FIGURE 24) reveals some latent inertia coupling as we can see the angle-of-attack erratically wobble in concert with sideslip and bank angle. [24] Our simulation follows pilot reports where he stated that he made sure to not provide any lateral inputs to the stick, δail==0º. Walker reported excessive lateral-directional oscillations that resulted in "bank angle changes from trim of about 20°" and did not stop until the angle of attack was brought down to α~2°. In order to observe the sort of response exhibited in flight, the initial conditions require β=8° ; if the simulation started with zero sideslip, roll rate and yaw rate, we saw no appreciable Dutch Roll motion.

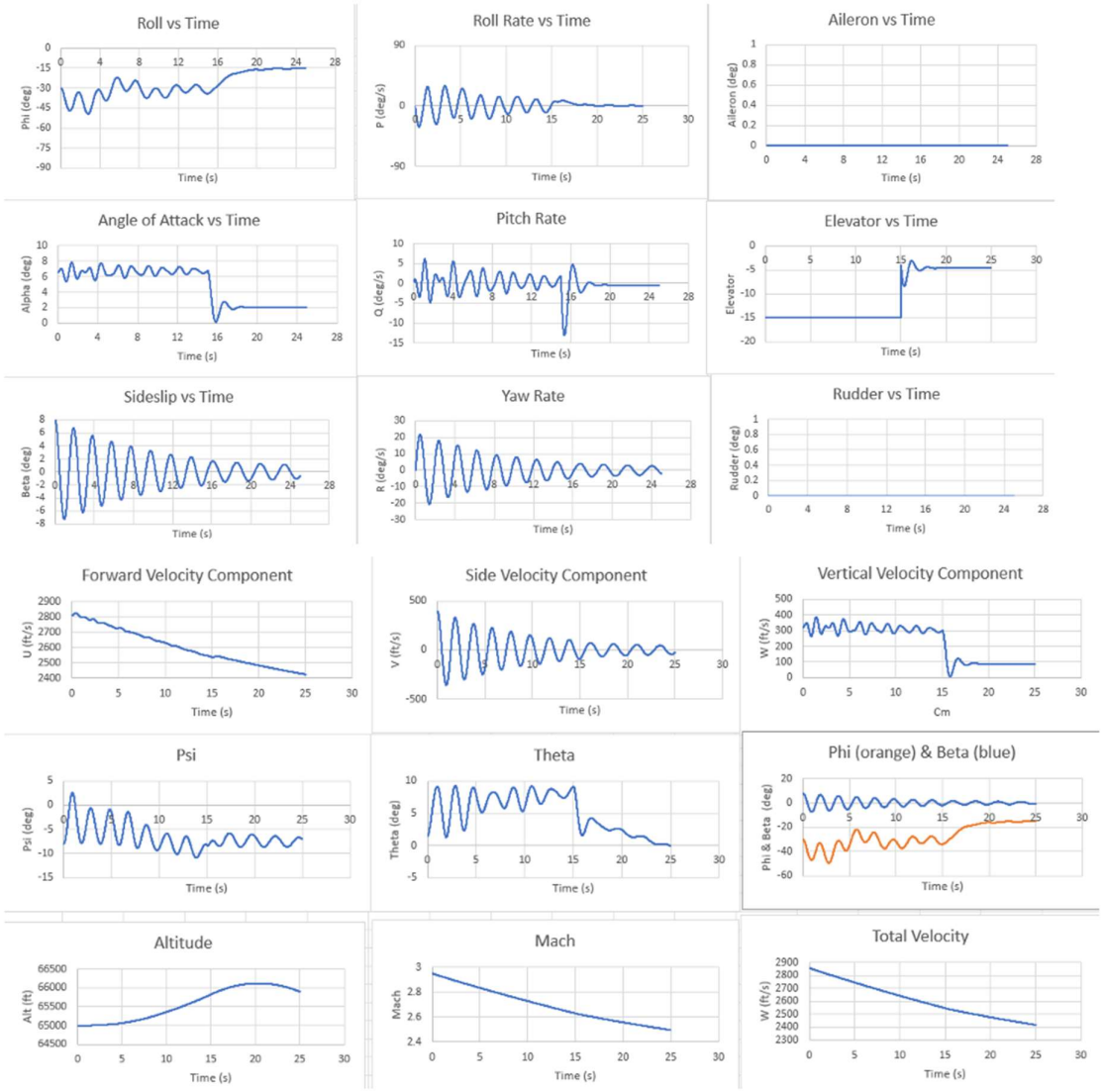


FIGURE 24 - Aircraft response during a turn with SAS settings at 4,0,0 for flight 1-11-21. note the poorly damped motions in pitch, roll, and yaw until the angle of attack is lowered to 2°

5. Summary & Conclusions

This work examined the stability and control characteristics of the early X-15-1 to learn more about the dynamic motions exhibited by slender high-speed aircraft with classical feedback control. It also documents the utility of rapid aerodynamic database generation, arising from panel-method computational aero tools, to broadly identify flying qualities problems and solutions. We compare bare-airframe and closed-loop simulator response of our model X-15-1 with vintage test pilot flight-test reports. We also compared bare-airframe and McRuer style "equivalent stability derivative" formulations to time-step integrating simulations. We can then assess our results in terms of MIL-STD-1797 quantitative handling qualities metrics.

We did not have sufficient preserved flight test data to perform a true parameter identification process across the entire aerodynamic database.

Using flight test cards from three different early X-15 missions, we determined the actual flight conditions for each test maneuver (speed, altitude, attitude, weight and mass moments of inertia). We could then recreate specific test conditions. We found that pilot's reports provided a consistent description of the simulated dynamic response of the aircraft. However, as flying qualities degrade – the simulator and pilot observed responses tend to differ more. Long term motions in the flight simulator became increasingly dependent on specifics of an out-of-trim starting conditions. Furthermore, the vortex-lattice derived aerodynamic database suggested more trouble with Spiral Divergence than reported by pilots. Within reason, a panel-method aerodynamic database is sufficient to make a strong attempt for initial feasibility and control law design.

Our simulations revealed the byproducts of strong Mach and angle-of-attack dependencies in the cross-coupling aerodynamic damping derivatives (Clr and Cnp) when running the time-dependent simulator with the roll damper is turned off; see Section IV.C. We saw throughout Section 4, that the X-15 demonstrated much better controllability, even when the associated dampers were turned off. While the aircraft did experience greater oscillations as Mach and angle of attack increased, they were not nearly as great or dangerous as compared to those experienced in the lateral direction. This is consistent with flight test experience, see Ref. [9].

The actual X-15 could experience Limit-Cycle-Oscillations arising from the SAS; see Ref [9][15]. Limit-Cycle-Oscillation's are self-sustained oscillations of constant frequency and amplitude that occur in non-linear systems. Due to rate and actuator limits, control surface effectiveness can be diminished to no longer operate in a linear fashion. Additionally, as gains are increased, and gain margin decreases, the control system becomes saturated and the possibility of experiencing these oscillations is increased [15] Because the as-flown actuator specifications have not survived to the present day, our time-step integration mode could not incorporate slew-rate and group-delay characteristics. Consequently, the present study could not be used to predict what gain setting would incite LCO.

6. Acknowledgements

Distribution Statement A. Approved for public release: distribution is unlimited. Docket # 88ABW-2025-0975 (Jan 8, 2026)

A special thanks to Karl Bender and his team at NASA/Armstrong Flight Research Center for clearing the 199 X-15 program flight test dockets for public release.

The views expressed are those of the authors and do not reflect the official guidance or position of the United States Government, the Department of Defense, the United States Air Force, or the United States Space Force.

7. Contact Author Email Address

Timothy.Takahashi@afit.edu

8. Copyright Statement

The authors are all employees of the United States Government, no copyright may be asserted on the original material included in this paper. We, the authors, confirm that this manuscript does not

contain any third-party material controlled by copyright (the archival material reproduced is also a work of the United States Government, since no copyright can be asserted it is in the Public Domain). We, the authors, confirm we grant permission for the publication and distribution of this paper as part of the ICAS proceedings or as individual off-prints from the proceedings.

References

[1] Miranda, L. R., Elliott, R. D., and Baker, W. M., “A Generalized Vortex Lattice Method for Subsonic and Supersonic Flow Applications,” NASA, CR 2865, 1977.

[2] Feagin, R. C., and Morrison, W. D. Jr., “Delta Method, An Empirical Drag Buildup Technique,” NASA, CR 151971, 1978.

[3] Drake, H.M., “Flight Experiences with Present Research Airplanes,” NACA X-15 Planning Conference, 1956.

[4] Jenkins, D. R., and Landis, T. R., “Hypersonic: The Story of the North American X-15,” Midland Publishing, 2003

[5] Anon., “Aerodynamic and Landing Measurements Obtained During the First Powered Flight of the North American X-15 Research Airplane,” NASA TM-X-269, Flight Research Center, Edwards Calif., 1960

[6] Alexander, M.G., “Subsonic Wind Tunnel Testing Handbook;” WL-TR-91-3073. United States Department of Defense WL/FIMM Wright-Patterson AFB, 1991. https://apps.dtic.mil/sti/tr/pdf/ADA240263.pdf

[7] Hoey, R. G., “Flight Planning and Conduct of the X-15 Envelope Expansion with Interim XLR-11 Rocket Engines,” AFFTC TDR-62-73, Air Force Flight Test Center, 1962.

[8] Flight Test Docket for X-15 Flight 1-5-10, NASA/Armstrong Flight Test Center, Edwards AFB, 1960. Declassified. Distribution Statement A.

[9] Tremant, R. A., “Operational Experiences and Characteristics Of The X-15 Flight Control System,” NASA TN-D-1402, Flight Research Center Edwards, Calif., 1962.

[10] Taylor, L. W. Jr., and Merrick, G. B, “X-15 Airplane Stability Augmentation System,” NASA, TN-D-1157, 1962.

[11] Souders, T. J., and Takahashi, T. T., “VORLAX 2020: Making a potential flow solver great again,” AIAA 2021-2458, Arizona State University, 2021.

[12] Takahashi, T. T., Griffin, J. A., Gaydusek, B. S., and Lorenzo, W. P., “VORLAX 2024: Further Upgrades to a Legacy Potential Flow Solver,” AIAA 2025-0848, Arizona State University, 2025.

[13] Saltzman, E. J., “Preliminary Full-Scale Power-Off Drag of the X-15 Airplane for Mach Numbers from 0.7 to 3.1,” NASA TM-X-430, Flight Research Center, Edwards, Calif., 1960.

[14] Taylor Jr., L. W., and Smith, J. W., “An Analysis of the Limit-Cycle and Structural-Resonance Characteristics of the X-15 Stability Augmentation System,” NASA TN D-4287, 1967.

[15] “Department of Defense Interface Standard: Flying Qualities of Piloted Aircraft (MIL-STD 1797A),” U.S. Department of Defense, Washington, D.C., 1990.

[16] “Military Specification: Flying Qualities of Piloted Airplanes (MIL-F-8785C),” U.S. Department of Defense, Washington, D.C., 1980.

[17] Rogers, H.B. “An Evaluation of X-15 Stability and Control Characteristics Using Legacy Flow Solvers, Historical Flight Tests, and Non-Linear Simulation to Replicate Aircraft Behavior,” M.S. Thesis. AFIT-ENY-MS-25-D-002, Air Force Institute of Technology, Wright-Patterson AFB, OH, 2025.

[18] Takahashi, T.T., Griffin, J.A., and Grandhi, R.V., “High-Speed Aircraft Stability and Control Metrics,” MDPI Aerospace, Vol. 12, 2025. https://doi.org/10.3390/aerospace12010012

[19] Yechout, T. R., Introduction to Aircraft Flight Mechanics, AIAA, 2024.

[20] McRuer, D.T, Graham, D. and Ashkenas, I., Aircraft Dynamics and Automatic Control, Princeton University Press, Princeton, NJ, 1973.

[21] Stein, G., "Respect the unstable," in IEEE Control Systems Magazine, vol. 23, no. 4, p. 12-25, Aug. 2003, doi: 10.1109/MCS.2003.1213600.

[22] Flight Test Docket for X-15 Flight 1-9-17, NASA/Armstrong Flight Test Center, Edwards AFB, 1960. Declassified. Distribution Statement A.

[23] Flight Test Docket for X-15 Flight 1-11-21, NASA/Armstrong Flight Test Center, Edwards AFB, 1960. Declassified. Distribution Statement A.

[24] Philips, W.H., “Effect of Steady Rolling on Longitudinal and Directional Stability;” NACA TN-1627, 1948.